

## Design and Demonstration of an Infrared Passive Ranger

*J. Patrick Reilly, Troy Klein, and Hillar Ilves*

**S**ome important targets can provide superior visibility in the infrared (IR) owing to thermal contrast. Current passive IR imaging systems designed for naval defense can yield highly accurate estimates of target angle, but not range data. This article describes the design and demonstration of a novel method for passively acquiring target range with an IR adaptation of an optical rangefinder. The concept uses a stereo perspective combined into a single lens and imaging camera. Tests with a laboratory prototype demonstrate that range error of only a few percent can be achieved at target ranges of 15 nmi or more, and with a stereo perspective baseline of 10 ft or less. One important attribute of the IR ranger is its completely passive nature; no energy is emitted to measure range and angular position. This could be especially important for certain military and surveillance applications. (Keywords: Infrared, Passive ranging, Rangefinder, Triangulation.)

### INTRODUCTION

Infrared (IR) systems, when used as part of a sensor suite on Navy ships, offer synergistic advantages for self- and area-defense purposes. Compared with radar, an IR sensor can achieve superior detection and tracking under conditions that can compromise radar performance, including electronic countermeasures, subrefractive radar propagation, high-velocity stealthy targets, heavy ducted radar clutter, radar multipath fades, and requirements for quiet electromagnetic radiation. In addition, an IR sensor can provide far better angle measurements of targets, which, when combined with known range, can yield highly accurate measures of target height. The consequent improved target height data could greatly facilitate the direction of weapons against a low-altitude target.

Conventional IR systems can furnish angle coordinates but not range data. The benefits of an IR sensor would be greatly enhanced if it could also measure range. To satisfy the objectives of a ship defense system, an IR system should determine range to a low-altitude target with an error of less than 10% out to the optical horizon (typically around 15 nmi).

The techniques described in this article were first developed under a 2-year independent research and development (IR&D) grant. We developed and analyzed concepts for IR passive ranging and performed several seashore tests with marine targets to assess various concepts and analyze problems. Subsequently, we constructed a laboratory test model of a passive ranger using optical registration as a prototype of the concept described here.

After demonstrating the feasibility of the passive ranging concept under IR&D funding, we received assistance from the Aegis program. Under Aegis support, we deployed an operational passive ranger test model at APL from which we gathered data on fixed and airborne IR targets, performed joint IR and radar tracking tests, and demonstrated an IR passive ranger capability that met all our requirements.

This article emphasizes the design and performance of an optical registration concept we initiated under IR&D support. We also include a brief description of two other approaches and their limitations.

## APPROACHES

We studied three solutions to the critical passive ranging problem of sensor alignment using (1) cross correlation of sea background imagery, (2) photogrammetry, and (3) optical alignment with a short baseline. All three approaches use triangulation to measure range once the alignment is determined.

Triangulation enables the determination of target range using two imaging IR sensors located along a known baseline (Fig. 1). If we know the baseline  $d$  and angles of arrival ( $\theta_1, \theta_2$ ) with sufficient accuracy, we can solve for the range  $R$  with simple geometric relationships:

$$\left(\frac{R}{d}\right)^2 = \frac{\frac{1}{2}\sin^2\theta_1 + \frac{1}{2}\sin^2\theta_2}{\sin^2(\theta_2 - \theta_1)} - \frac{1}{4}. \quad (1)$$

The range error  $\Delta R$  depends on the range, the effective length of the baseline, and the angle errors,  $\Delta\theta_1$  and  $\Delta\theta_2$ , of each sensor. If the angle errors are random and statistically independent, and they have the same variance, the fractional range error<sup>1</sup> is

$$\frac{\sigma_{\Delta R}}{R} = \frac{\sqrt{2}\sigma_{\Delta\theta}R}{d|\sin\theta|}, \quad (2)$$

which is valid for  $\theta \approx \pi/2$  and  $R/d \gg 1$ ;  $\sigma_{\Delta R}$  and  $\sigma_{\Delta\theta}$  are the standard deviations of the range and individual

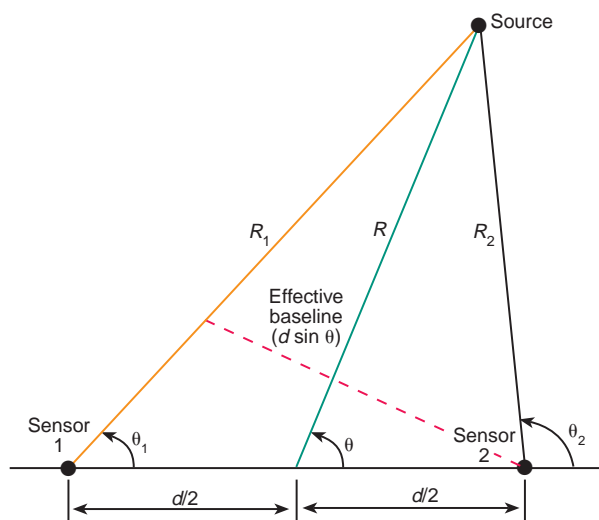


**Figure 1.** Passive ranging geometry ( $R$  = range,  $d$  = baseline,  $\theta$  = angle of arrival).

sensor angles, respectively. The expression is illustrated in Fig. 2 as a function of the aspect angle for a baseline of 100 ft. The denominator of this expression shows that the effective baseline varies as  $\sin\theta$ .

Notice in Eq. 2 that the range error is inversely proportional to the baseline length. Therefore, when trying to reduce range error, it is desirable to use the longest baseline possible. The parameter  $\sigma_{\Delta\theta}$  is the root-mean-square error used in determining the individual angles of arrival at the two sensors ( $\theta_1, \theta_2$ ). In practice,  $\sigma_{\Delta\theta}$  would include both the uncertainties of measuring the angular position of the target with respect to the individual sensors and the uncertainty of the sensor pointing angles themselves. With a long baseline ranging system, this latter uncertainty is especially significant, considering two sensors separated by 100 ft on a flexing ship structure. Consequently, to support such a system on a ship, we must correct for the misalignment of the two sensors dynamically. The problem of measuring sensor misalignment in such a system makes the implementation of a passive IR ranger difficult.

## Sea Background Imagery

Our original concept for shipboard IR ranging was to place a pair of sensors fore and aft at a separation of about 100 ft to accommodate targets at aspect angles down to  $30^\circ$  or so from broadside (giving an effective baseline of at least 50 ft) and another pair on a smaller orthogonal baseline to handle the remaining aspect angles. For this approach, we investigated a method of

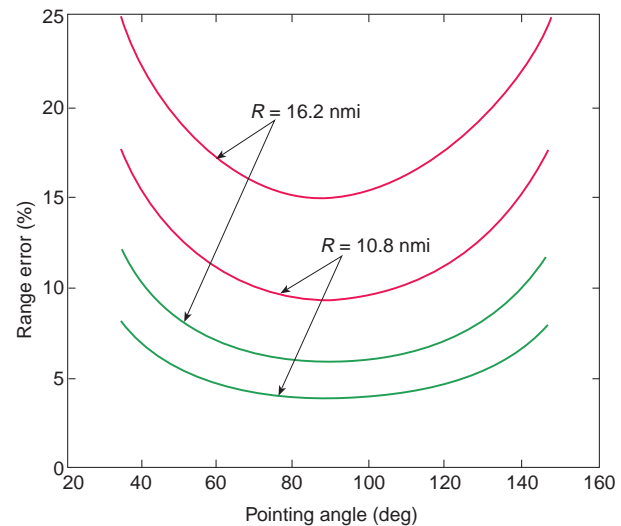


**Figure 2.** Range error using triangulation with a 100-ft baseline. Pointing angle indicates target position with respect to baseline at midpoint; errors for angle of arrival are statistically independent. For red curves, the standard deviation of the sensor angle ( $\sigma_{\Delta\theta}$ ) = 100  $\mu$ rad; for green,  $\sigma_{\Delta\theta}$  = 50  $\mu$ rad.

dynamic sensor registration using a cross correlation of sea background in the two images,<sup>1</sup> eventually leading to an invention disclosure.<sup>2</sup> This method utilizes the fact that an IR image of the sea consists of contrast features that result principally from variations in the reflectance of sky radiation at IR wavelengths as well as temperature variations on the surface of the sea. The effect resembles a visual image of the sea, in which the eye detects a pattern of individual waves made visible by sky reflectance.

Our cameras, having a noise equivalent temperature difference (NE $\Delta$ T) of only 25 mK, can detect extremely small variations in source irradiance. NE $\Delta$ T indicates the required temperature difference of a particular pixel with respect to the background to obtain a signal-to-noise ratio (SNR) of unity. With this fine degree of sensitivity, we readily observe wave-size spatial features of the sea in the IR band, even at relatively low sea states during the night.

The sea registration process requires that the spatial coordinates of sea features are first corrected for the parallax existing in the images of the two cameras. For this process the range to the features must be known. One can determine range to a feature on the surface of the sea with a simple geometric calculation by knowing the height of the sensor and the relative elevation angle of the feature with respect to the horizon. To implement this technique, one must accurately determine the horizon in the image formed by at least one of two cameras. After correction for parallax, the images from both cameras are cross correlated. The position of the cross-correlation peak reveals the differences in pointing angles of the two cameras, information that is essential to the triangulation calculation.

We conducted tests with low-altitude marine targets viewed by two cameras laterally separated by 100 ft and elevated above the sea by 90 ft (the expected height of shipboard sensors). Data were collected under a variety of atmospheric conditions in which the range of a controlled test target equipped with a Global Positioning System (GPS) varied from about 1 nmi to the limit of the optical horizon. The images acquired in these tests were processed in the laboratory.

Results revealed that relative pointing angles of the cameras could be determined to a precision of less than 1 pixel through image cross correlation.<sup>1</sup> To achieve this accuracy, it was necessary to locate the horizon with great precision. Our measurements showed that one cannot always do this with IR imagery. The horizon is not always visible to the IR camera, and it may be difficult to distinguish the true horizon from stratified sea or cloud features that may appear as a "false horizon." Furthermore, atmospheric refraction can perturb the apparent position of the horizon. Because

these problems are not easily overcome, we decided to investigate other alternatives.

### Photogrammetry

The concept of photogrammetry for determining the range to features in visual imagery is hardly new. Indeed, a patent for this technique was awarded in 1893. The concept was developed during the Civil War to determine the positions of troops using photographs taken from elevated balloons. Photogrammetry requires one to identify common objects and their relative positions in each of two images obtained from separated sensors. The relative positions are applied to a set of equations to solve for several unknowns, including sensor position, pointing angle, and the locations of the objects in the image.

In our application, we assumed that the lateral separation (baseline) of the sensors and the focal length of the cameras would be known with sufficient accuracy. Unknowns would include the pointing angles of the cameras with respect to a common reference and the ranges of the objects in the image. In principle, one should be able to solve for all remaining unknowns with only five common reference sources. Once the relative pointing angles of the cameras are determined, it should be possible to obtain the ranges to all objects in the image.

The concept of photogrammetry appeared to have merit for our problem. We reasoned that reference objects could include friendly or hostile air and sea targets. In addition, one might be able to position reference IR sources by means of small rocketry, or perhaps use natural sea or land background features.

To investigate the concept, we conducted experiments in which two IR cameras were placed on a baseline of 100 ft. Reference IR sources were placed on the roofs of APL buildings within a field of view (FOV) common to both cameras. A controlled helicopter (containing GPS) provided a target source at various known ranges.

Results of the photogrammetry study<sup>3</sup> showed that acceptable accuracy was not possible unless the FOV was unrealistically large, i.e., 20° or more, in contrast to an FOV of 2° available in typical IR cameras having acceptable resolution. Although fields of regard approaching 360° are available in scanning IR search systems, it would be difficult to maintain the azimuth registration to subpixel accuracy over that range. In addition, a ship-mounted platform provides an oblique viewing angle of the scene rather than the near-nadir viewing angle from an airborne platform for which photogrammetry was developed. This severe observation angle with surface sensors makes the photogrammetry equations unstable and difficult to solve numerically.

## Optical Alignment

Considering the difficulties with the two previously described methods, we decided to more actively pursue a method for IR ranging using the optical alignment of two sensors. A derivative of this method not only proved to be feasible, but we were able to demonstrate acceptable ranging accuracy with a baseline of 10 ft or less—and with a single camera.

Figure 3 illustrates the range computation concept used in the optical alignment method. Two cameras are depicted along a baseline  $d$ . To simplify the illustration, an IR source is assumed to be aligned with the optical axis of camera 1, although a more symmetric view of the target along the centerline of the baseline would be likely. A small baseline allows the device to be steerable, and baseline shrinkage due to off-axis angles of the target, as in Fig. 1, is not a concern. The image of the target in camera 2 will be formed at a slightly different angle on the focal plane. If the cameras are perfectly aligned, we can imagine that both images are represented on a single focal plane as represented at camera 2.

By geometric relationships involving similar triangles in Fig. 3, we derive the expression

$$R = \frac{df}{s}, \quad (3)$$

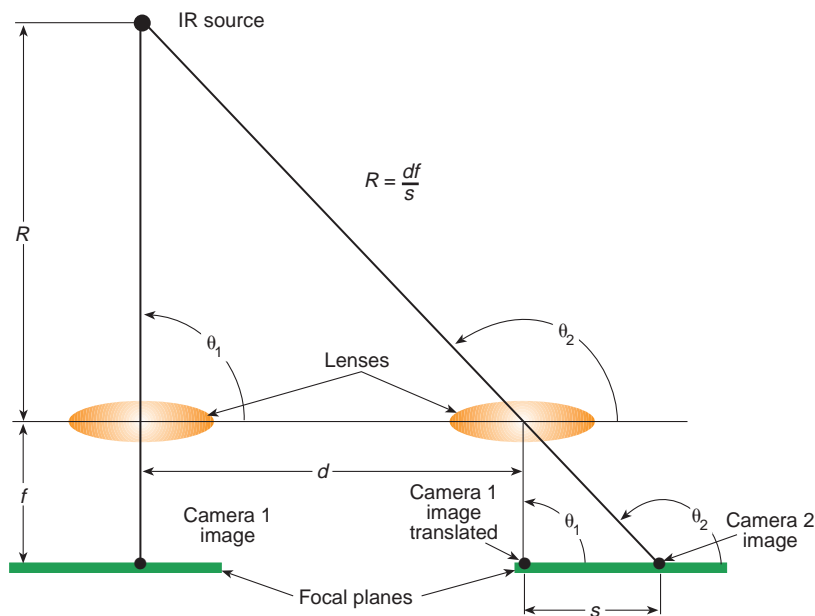


**Figure 3.** Range computation concept:  $R = df/s$  ( $R$  = range to target,  $d$  = baseline,  $f$  = focal length of the lens,  $s$  = image separation on the focal plane, and  $\theta$  = angle of arrival).

where  $R$  is the range to the target,  $f$  is the focal length of the lens, and  $s$  is the image separation on the focal plane. Equation 3 is related to Eq. 1 through a series of approximations. To illustrate this relationship using parameters typical of our system, with  $f = 560$  mm and  $d = 3$  m, a target range of 20 km would produce a focal plane image separation of  $s = 84 \mu\text{m}$ , which is roughly the distance across 2 pixels in the focal plane array.

So far we have discussed a simple triangulation concept. As with other methods that we investigated, a major challenge is to determine and correct for the pointing angles of the two cameras. With a small baseline, the cameras are easily within optical view of one another, and we could employ optical techniques to measure and subsequently correct for camera misalignments. We have achieved the equivalent effect with a unique optical design described in the next section.

## IR PASSIVE RANGER DESIGN

The basic optical layout of the IR passive ranger that we eventually implemented is illustrated in Fig. 4.<sup>4</sup> In place of two cameras, we have used two mirror assemblies called “pentamirrors.” (Pentamirror is a term derived from the optical “pentaprism,” which is a solid prism having five sides in one cross section. Although the pentamirror bears little resemblance to a pentaprism, the name has been applied because of its similar function.)

The pentamirrors acquire energy from two perspectives along a baseline and direct that energy to a single lens and camera assembly. This results in a double image on the focal plane, a concept similar to one used in military and commercial visible-wavelength range finders. So that the energy from pentamirror 1 is not blocked by pentamirror 2, the mirror assemblies are offset one above the other, each using half the aperture of the lens.

The pentamirror deflects energy at a  $90^\circ$  angle as shown by the inset in Fig. 4. Mirror faces are oriented at a  $45^\circ$  angle. The ray paths are insensitive to rotations of the pentamirror about the  $z$  axis perpendicular to the page.

Because of the property of rotational insensitivity, the positions of the images in the focal plane in Fig. 4 are insensitive to the rotation of the individual pentamirrors about

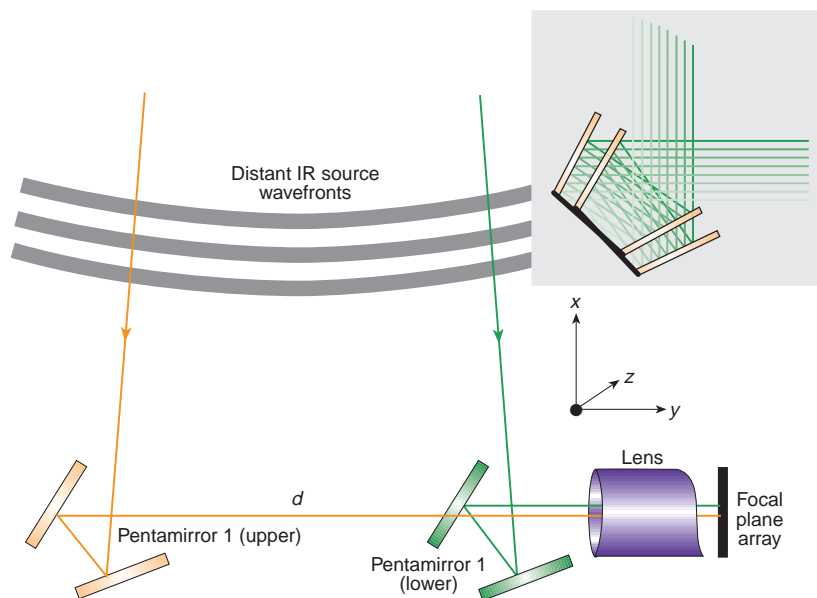


**Figure 4.** Optical layout of the IR passive ranger. Inset shows invariance of ray deflection to rotation of pentamirror about an axis perpendicular to the page ( $z$  axis).

their respective  $z$  axes or to flexing of the ranger along a line comprising the baseline. This property removes the major source of error in a ranger that uses the principle of triangulation, namely, uncertainties in the pointing angles of the two viewing devices. A secondary source of error does remain if there is rotation about either the  $x$  or  $y$  axis of Fig. 4, although it is not significant for a reasonably rigid baseline structure.<sup>5</sup>

For the system shown in Fig. 4, the two images of an IR source at nominal ranging distances would partially overlay one another on the focal plane. To separate the target images, one pentamirror is modified so that the ray deflection angle is somewhat less than  $90^\circ$ . In our implementation, we accomplished this by offsetting one reflector surface by approximately  $0.1^\circ$ .

Although the total images from the two perspectives remain superimposed, the pentamirror offset shifts one image relative to the other, such that the simple test target images are unambiguously separated. In an optimum design, to accommodate a complex multiple target environment, it would be preferable to completely separate the full image fields on the focal plane so that they are side by side without superposition. The ranger calibration accounts for the pentamirror offset of the two images.

Figure 5 illustrates the passive ranger test assembly at APL as it was configured with a 10-ft baseline. This ranger was oriented vertically on an illuminator pedestal on the roof of Building 40. The pedestal, part of the Aegis Mk-99 Fire Control System, is a stabilized two-degree-of-rotational-freedom (train and elevation) platform. In other tests, the ranger baseline was oriented horizontally. The vertical configuration offers

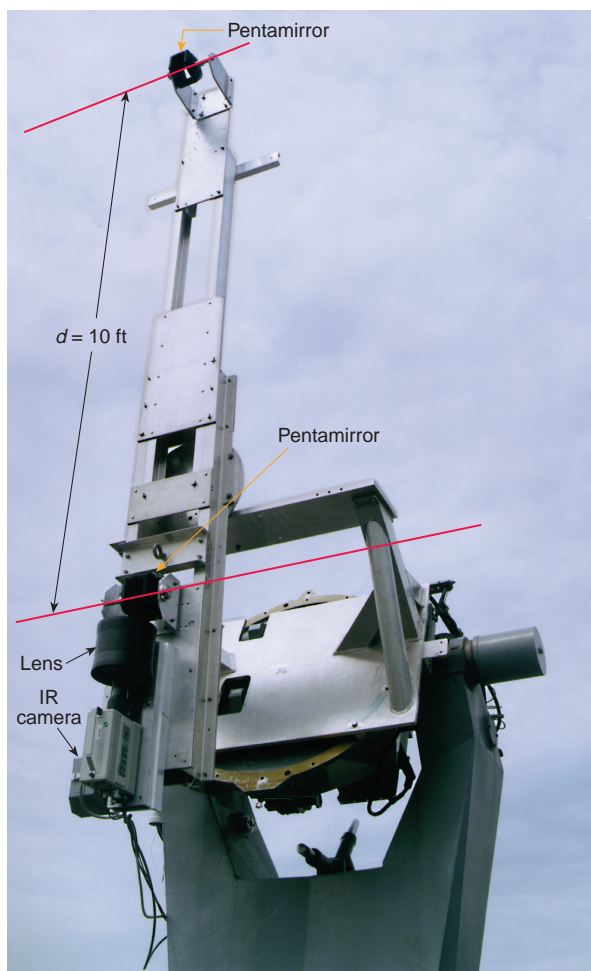


**Figure 5.** Passive ranger test unit, in a vertical configuration, mounted on an Mk-99 illuminator pedestal. The baseline  $d$  is the distance between the pentamirrors.

certain mechanical advantages, since the device can be steered in azimuth with a smaller moment of inertia than with a horizontal baseline. However, the vertical baseline introduces an additional error due to the vertical refractive structure of the lower atmosphere (discussed in a later section). Consequently, most of our tests were conducted with a horizontal baseline, as shown in Fig. 6. In this photograph, one can appreciate the scale of the ranger compared with the AN/SPG-55B C-band radar.

Characteristics of the camera and lens are given in Table 1. The camera has a focal plane array with  $256 \times 256$  elements. Ranging tests were conducted with a 560-mm



**Figure 6.** IR passive ranger test unit under installation in a horizontal configuration adjacent to the AN/SPG-55B radar.

lens with both reflective and refractive elements. The FOV was  $1^\circ$ ; the instantaneous FOV (IFOV) or pixel resolution was  $68 \mu\text{rad}$ . The pentamirrors are high-precision surplus units from Poseidon submarines.

The output from the camera consists of a series of digital frames. Images are conveyed by cable to a remote data acquisition system. Processing of the images, including the determination of range, is now done in the laboratory after the tests; we plan to automate on-line programs for real-time processing in a future prototype unit.

Our ranger design eliminates or greatly ameliorates several major sources of error, which are discussed in detail in the next section. The use of pentamirrors makes the system nearly insensitive to rotations, twisting, or vibrations that cause errors in the triangulation calculations—a significant source of error that would otherwise be present. The use of a single camera and focal plane eliminates errors that would otherwise be present with two sensors. In contrast to our design, a two-camera system would require precision alignment of two focal plane arrays, time correlation of the two images, image scaling for optical focal length differences,

**Table 1. Camera and lens characteristics.**

Item	Description
Camera	Amber Radiance I, focal plane array
Waveband	3–5 $\mu\text{m}$
Pixels	256 $\times$ 256
Frame rate	60 Hz (max.)
NE $\Delta$ T	25–35 mK
Quantization	12 bits
Detector width	31 $\mu\text{m}$
Detector spacing	38 $\mu\text{m}$
Focal length <sup>a</sup>	50, 75, 100, 250, and 560 mm
IFOV	760, 507, 380, 152, and 68 $\mu\text{rad}$
FOV	10, 7, 5, 2, and $1^\circ$
Aperture diameter	5, 10, 8, 10, and 20 cm

<sup>a</sup>Five different lenses were available; we used the 560-mm focal length, with corresponding IFOV and FOV.

and correction for focal plane array vibrations and shifts.

## SOURCES OF ERROR

The precision requirements for some of the ranger elements are demanding. One can appreciate the sensitivity to separation angle errors with reference to Fig. 7, which shows the pixel separation of the two images from a point target at various ranges. For instance, for targets at 11 and 20 nmi, separations are about 2.2 and 1.2 pixels, respectively. Thus, an error of 1 pixel applied to a target at 11 nmi would result in a 9-nmi range error.

The inset in Fig. 7 illustrates range error as a function of range for a 10-ft baseline-steerable ranger, i.e., one that can maintain the baseline nearly perpendicular to the target direction. Note that at a range of 10 nmi, a separation angle error of 15  $\mu\text{rad}$  (0.22 pixel) results in a range error of about 9%. Clearly, to achieve acceptable range accuracy, one must determine the relative angular separation of the target images with an error less than 1 pixel. Various sources contribute to relative angle errors, as we discuss in the following paragraphs.

### Lens Distortion

Because of imperfections in the lens optics, the image on the focal plane may be distorted. In a good-quality lens, such distortions are typically so small that they cannot be detected by the eye. However, with the demands of accuracy on our system, even small errors can be important. To overcome these potential error sources, the distortions that occur across the focal

plane must be mapped. Figure 8 is such a map produced through laboratory measurements of our lens and camera.<sup>6</sup>

The approach is to use a device that can precisely control the pointing angle of the camera and lens to measure how the lens images a fixed target. A comparison is then made between the measured results and those expected from a perfect lens. The differences are modeled with two-dimensional polynomial equations, which provide a means of resampling distorted images into images without distortion. Therefore, imagery from the camera can be corrected to appear as if it were imaged by a perfect lens.

The vertical axis in Fig. 8 indicates the distortions (in pixel units) of a point source at infinity with respect to a perfect lens and camera. In the central part of the lens, the distortions amount to a fraction of a pixel; however, for an image near the periphery of the FOV, the error can amount to several pixels. As suggested by Fig. 7, such errors can result in unacceptably large range errors.

To preserve the validity of the distortion measurements, the design of the camera and lens mounts is critical: whenever the lens and camera are separated and rejoined, they must be placed in exactly the same relative position. Furthermore, the lens must be inflexible with respect to the camera. This requires a very rigid mounting method.

### Pentamirror Thermal Effects

Recall that pentamirrors were introduced to the ranger to eliminate the need for sensor misalignment measurements. This improvement is effective only if the pentamirrors continue to reflect images through the

intended angles. If some factor were to cause the reflector angles within the pentamirrors to vary, a target separation angle error would result.

A thermal gradient across the structure of the pentamirror is one factor that could change the reflection angle. We discovered this during ranging tests, when one side of a pentamirror was illuminated by the Sun and another side was in shadow. In those tests, the system required calibration about every 10 min. To confirm the source of the calibration drift, we performed laboratory tests in which a radiative heat source was directed to one side of a pentamirror, causing a thermal gradient of about 10°C across the mirror housing. Relative mirror alignment could

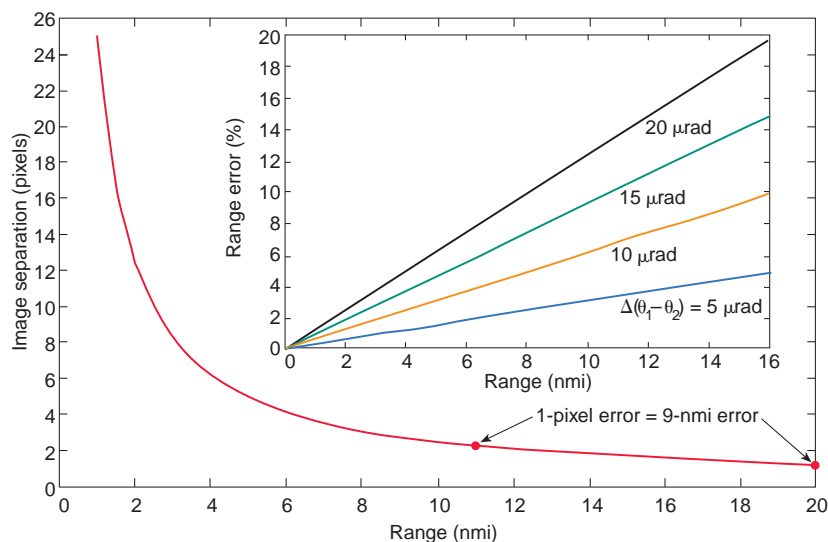


**Figure 7.** Image pixel separation as a function of target range. Focal length = 560 mm; baseline = 10 ft. Inset shows predicted range accuracy for a steerable 10-ft baseline system. At 10 nmi, a separation angle error of 15  $\mu\text{rad}$  yields a range error of about 9%.

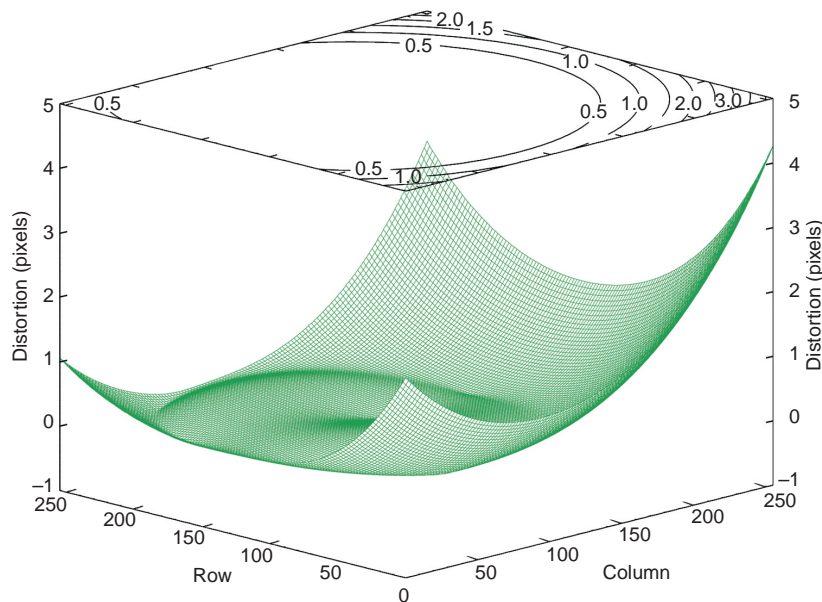


**Figure 8.** Distortion map for the 560-mm lens. The vertical axis indicates the distortions (pixel units) in the location on the focal plane of an image of a point source at infinity with respect to a perfect lens.

be measured with an autocollimator to a precision of about  $30 \mu\text{rad}$ . We found that this sort of thermal gradient resulted in offset variations similar to those found in the outdoor tests.

To avoid thermal gradient problems, mirror assemblies must be shielded from solar radiation or other thermal sources. In a future design, we plan to place the optics in an air-conditioned housing. Gradual temperature changes should not be a problem: if the housing is made from a single material and maintains a uniform temperature, it would expand or contract uniformly in all dimensions, and relative angles would be maintained.

### Angular Cross-Coupling Errors

The accuracy of the passive ranger degrades with errors in the angular difference ( $\theta_1 - \theta_2$ ) (inset, Fig. 7). Without the pentamirror design,  $\Delta\theta$  errors would result from any rotational motion of the optics about the  $z$  axis (Fig. 4); with the pentamirrors, these rotations are removed as a major source of error. There does, however, remain a small residual error if the optics rotate about either of the other two axes. Any rotation of the optics about the  $x$  or  $y$  axis will couple into the difference angle,  $\theta_1 - \theta_2$ , that is used to determine the range. By using an optical design software package and laboratory measurements,<sup>5</sup> we determined that the errors were acceptably small for rotations of less than 1 arcmin. Although the first-generation prototype ranger cannot achieve 1-arcmin stability, future versions will have more rigid baseline structures with sufficient stability.

### Refractive Turbulence Effects

Scintillation and angle of arrival variations are phenomena in which propagated energy is affected by fluctuations in the index of refraction of the atmosphere—largely as a result of temperature fluctuations. These temperature variations occur through turbulence of the atmosphere caused when moving air interacts with the surface of the land or sea. Such variations result in fluctuations of the amplitude of the source (as with the twinkling of stars, referred to as scintillation) and changes in the angle of arrival of the energy. Both effects can impact ranging performance. Amplitude scintillation can affect performance because it can cause the target signal on one or both images to fall below an acceptable SNR at a particular instant of time. The angle-of-arrival variation is random and operates independently on both images, thereby causing a separation angle variation and ranging errors.

The theory of IR scintillation and its application to IR search and track systems has been investigated in previous work.<sup>7,8</sup> This theoretical framework was applied to the angle errors in the passive ranger.<sup>9</sup> In Fig. 9, the predicted range error as a function of range, turbulence, and receiver aperture is shown. The values plotted assume 16-point averaging of the data to be compatible with ranging accuracy measurements presented later in this article. Assuming independent samples, temporal averaging reduces angle-of-arrival errors by the square root of the number of data points

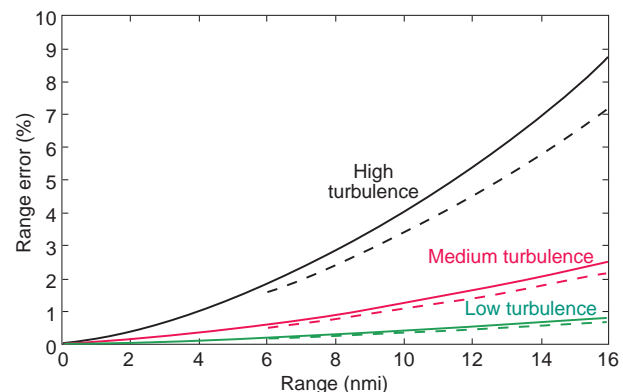


**Figure 9.** Range error due to refractive turbulence and aperture size, with 16-point averaging assumed (solid curves, 3-in. aperture; dashed curves, 8-in. aperture).

averaged because the angle variation is a random process. The correlation time of angle-of-arrival fluctuations is sufficiently short (typically 20 ms, depending on environmental conditions) for the averaging discussed here.<sup>9</sup> The larger receiver aperture reduces range errors due to an angle-of-arrival spatial averaging effect. When the predictions shown in Fig. 9 are compared with measured ranging results, it appears that a significant portion of the observed ranging error may be attributable to refractive turbulence effects.

### Differential Refraction with Vertical Baseline

In addition to the small-scale refractive index variation described in the previous section, a larger-scale variation exists with altitude. This vertical stratification in the atmosphere causes the propagation path of electromagnetic radiation to curve in a vertical plane. The amount of curvature depends directly on the vertical gradient of refractive index at that point. In general, propagation rays will bend toward Earth. Some environmental conditions may cause them to curve away from the surface or even become trapped in a duct. Refractive variations associated with the stratified atmosphere do not vary rapidly with time, and the associated angular deviations cannot be mitigated by temporal averaging.

Stratified refractive variations can cause significant errors in a passive ranger with a vertical baseline.<sup>10</sup> An important property of the Standard Atmosphere is that the vertical refractive index gradient is constant with altitude; that is, two rays that propagate at two different altitudes will experience the same amount of curvature. Therefore, the rays that propagate to each receiving point of a vertical ranger will have curved by the same amount, preserving the angular relationship required for ranging. If, instead, the atmosphere has a nonuniform vertical refractive index gradient, then the two rays will be bent by differing amounts (“differential refraction”), thereby introducing ranging errors. A horizontal baseline ranger is not subject to these errors because the critical angles of the ranging triangle are perpendicular to the refractive ray curvature.

Through the use of an atmospheric ray trace model and experimental measurements, differential refraction was found to dramatically affect the ranging accuracy of a vertical baseline ranger.<sup>10</sup> The ranging errors can be as much as 100%; even negative range estimates can result. Since the atmosphere is rarely or never “standard,” these errors must be seriously considered.

Angle-of-arrival errors from vertical refractive layers could, in principle, be corrected if the structure of the lower atmosphere were known in sufficient detail. However, the degree of detail required and methods for correction have yet to be determined. Until we better

understand these issues, we consider it advisable to configure a passive ranger with a horizontal baseline.

### Subpixel Image Location

To determine target range with desired accuracy, the position of a target’s image must be determined to an accuracy of less than 1 pixel. Any error in target position will directly result in range estimate errors. Two methods for measuring target position have been used to date, centroiding and cross correlation. Although both methods have advantages and disadvantages, the preferred approach is cross correlation. Both methods require sufficient target signal strength to be effective. Experimental measurements indicate that targets with an SNR of approximately 7 dB or more are suitable for ranging with our system.

Subpixel centroiding allows energy from even a point target to spread across several pixels in the focal plane. The distribution of energy, described by a point spread function, is affected by diffraction and, more importantly, imperfections in the optics. In our optical system, the most significant amount of energy from a point source is spread over a field of about  $3 \times 3$  pixels; the distribution of energy over those 9 pixels depends on the precise location of the target within the field. The centroid is essentially a center-of-energy calculation using the energy distribution on the focal plane. Only energy above a threshold can be used to reduce the impact of background noise in the image. The value of the threshold must be carefully chosen for best results.

We select the threshold dynamically, such that a predetermined number of pixels is used for the centroid calculation. Centroiding works well for compact, point-like targets, but not for larger targets that have dimensions of 5 pixels or more. Different portions of large targets tend to vary in intensity with time, which results in centroid errors. An important advantage of centroiding is the relatively simple calculation involved, which would benefit a real-time ranging system that must process data at a high rate of speed.

For the cross-correlation method, two identically sized rectangular subimages of each target image are selected; their original location in the full image is recorded. The subimages are spatially upsampled by a factor of 10 using nearest-neighbor or bilinear interpolation. The spatial cross-correlation function of the upsampled images is then computed. The location of the peak correlation, in addition to the original offset of the two subimages, gives the angular target separation needed for range calculation. This method has several advantages over the centroiding method: no threshold determination is required; the target location accuracy does not degrade with target size; and the method tolerates over- or underresponsive pixels very

well. Unfortunately, the cross-correlation calculation requires significantly more computing than the centroid calculation. Nevertheless, we use the cross-correlation method because it is more robust than centroiding and we do not presently require "real-time" processing.

### Focal Plane Movement

For our camera, the location of the focal plane with respect to the camera body varies with time. In laboratory tests, changes in position appeared to be random, with occasional sudden jumps of several tenths of a pixel to a new position. We hypothesized that these variations were due to small temperature changes of the cooled focal plane array, although this conjecture remains unproven. The manufacturer has indicated that, because of the extreme temperature differences experienced by the array (and its associated expansion and contraction), it is allowed to float within its mount, thereby causing the motion observed in our tests. Such variations would be inconsequential for most applications but can be significant for a passive ranging system that uses two cameras. These position variations, however, are unimportant if one uses a single camera and focal plane, as we do. In this case, the position change is the same for both images, such that the angular difference of a target image is preserved.

## DATA PROCESSING

A significant amount of data processing is required for the passive ranging system. The first step is data acquisition. The IR camera provides 12-bit digital imagery at 60 frames per second. The data are transferred to a desktop computer in 16-bit words for recording. The computer has two modes of image acquisition: burst and continuous. In burst mode, up to 109 images can be collected into random access memory at the full rate of 60 frames per second. The computer then requires about 1 min to save the imagery to disk. In continuous mode, which we routinely used for the tests described in this article, the computer records about 2 frames per second directly to disk. (For future testing, recently acquired hardware will increase the continuous frame rate to more than 10 frames per second.) In addition to recording the imagery, each image is tagged with the computer time at the instant it is acquired. The acquired data are then transferred to Exabyte tape for off-line processing in the laboratory.

The next step is to process the imagery to determine angular target separation. The imagery must be resampled to remove lens distortion as described in a previous section. Images are then appropriately amplitude-scaled to make the target visually apparent

if present. Once the double target images are manually identified in each image using a graphics display, a region-of-interest rectangle is manually positioned around each target image. These selected regions are then centroided or cross correlated to determine angular separation. The angular separation data are tabulated along with time and frame number information.

The ranging system must then be calibrated. Using a subset of the angular separation data for a target at known range, the system calibration angle can be determined. The calibration angle is then used to calculate range for the remaining data. Once the range is calculated, it is examined graphically and statistically for accuracy.

Since many of the error sources that contribute to ranging error are random, a 16-point moving average is applied to the data to reduce the error by approximately a factor of 4. More than 16 points could be averaged, but at the rate of 2 frames per second, the process would encompass data from an excessive time extent. (Two frames per second was the highest rate our data collection equipment could sustain.) The new higher-rate image acquisition hardware will allow more averaging to be applied without extending over a large range in time.

In a future ranging system, we will focus much of our development efforts on performing the data processing automatically and in real time.

## EXPERIMENTAL RESULTS

Having constructed the experimental ranging test unit (Figs. 5 and 6), we performed a series of ranging accuracy tests. An initial series of experiments was conducted with the unit located on the roof of Building 6 at APL; subsequent tests were conducted jointly with radar tracking from the roof of Building 40.

### Fixed-Location Target Tests

The passive ranger was initially mounted on a surplus machining rotary table that could be steered over limited azimuth and elevation sectors. From its rooftop position, we could range on a variety of cultural features including water towers, microwave towers, and buildings. We also surveyed locations where we might position a controlled test target. We hoped to find positions from which target ranges could vary from 2 nmi to at least 15 nmi. Our initial surveys showed that it would be extremely difficult to access suitable locations for a target, since visibility at ground level was hampered by intervening trees and other obstructions.

We decided to use flares and model rockets as IR sources. These devices produced an IR signature similar to a real target. We could identify locations at

acceptable ranges from which we were permitted to launch the targets. The launch locations were accurately surveyed using GPS. Communication was maintained via cellular phone between the launch and measurement stations. Just before launch, the cameras were activated to begin collecting frames of images. As the IR sources gained altitude, they became visible above the obstructing trees.

Figure 10 illustrates multiple, superimposed frames of a flare and rocket at a distance of about 5 nmi. The lower parts of the images consist of trees. One can see a series of images from each of the two mirrors overlaid on a single picture. Note that the flare appears to break into two major pieces after apogee.

Figure 11 shows a magnified picture of several targets, including a calibrated 20-in.-dia. source heated to 137°C and at a distance of 3.2 nmi. Also shown are signatures of a 500-W quartz lamp, magnesium flare, and model rocket. The quartz lamp was used in air target tests described next.

The plots in Fig. 11 are read as follows. On the outside of the darkened image, one sees a small arrowhead on the top and left-hand borders. The plot on the right-hand side represents detector readouts along a vertical line aligned with the upper arrow. The lower plot represents the readouts along a horizontal cut aligned with the left-hand arrow. The arrowheads have been positioned so as to include the brightest pixel in each cut. The vertical axes of the plots show digital detector "counts," which are proportional to the energy accumulated in a detector integration period. Considering target range, the four signatures in Fig. 11 are similar.

These experiments were valuable for proving that IR passive ranging is feasible and that a variety of IR sources can be used. Unfortunately, the amount of ranging data for these targets was limited by fixed distances and short flight times.

### Airborne Target Tests

We conducted a second series of tests using airborne targets and an AN/SPG-55B radar (Fig. 6). The IR ranger was installed on an Mk-99 illuminator pedestal, which was slaved to the radar to maintain targets within the IR FOV.

IR sources consisted of targets of opportunity (airliners, business jets, small aircraft, helicopters) flying through the Baltimore/Washington corridor and a controlled Cessna aircraft. Figure 12 shows an example of a double image of a jet (at a 9-nmi range) used for ranging measurements. Notice that the outline of the aircraft is visible in addition to the hot engines. Not all airliners exhibited this signature; often, the IR intensity of the engines did not significantly differ from the rest of the aircraft.

The Cessna provided a visible IR signature from the hot engine at approaching and crossing aspects. However, for outbound aspects, its signature was not sufficient for our purposes. To augment the signature, a passenger in the Cessna positioned a 250-W quartz lamp to be visible from APL.

During tests, IR data were collected at the rate of 2 frames per second. Simultaneously, we recorded radar tracking data consisting of target range, azimuth, and

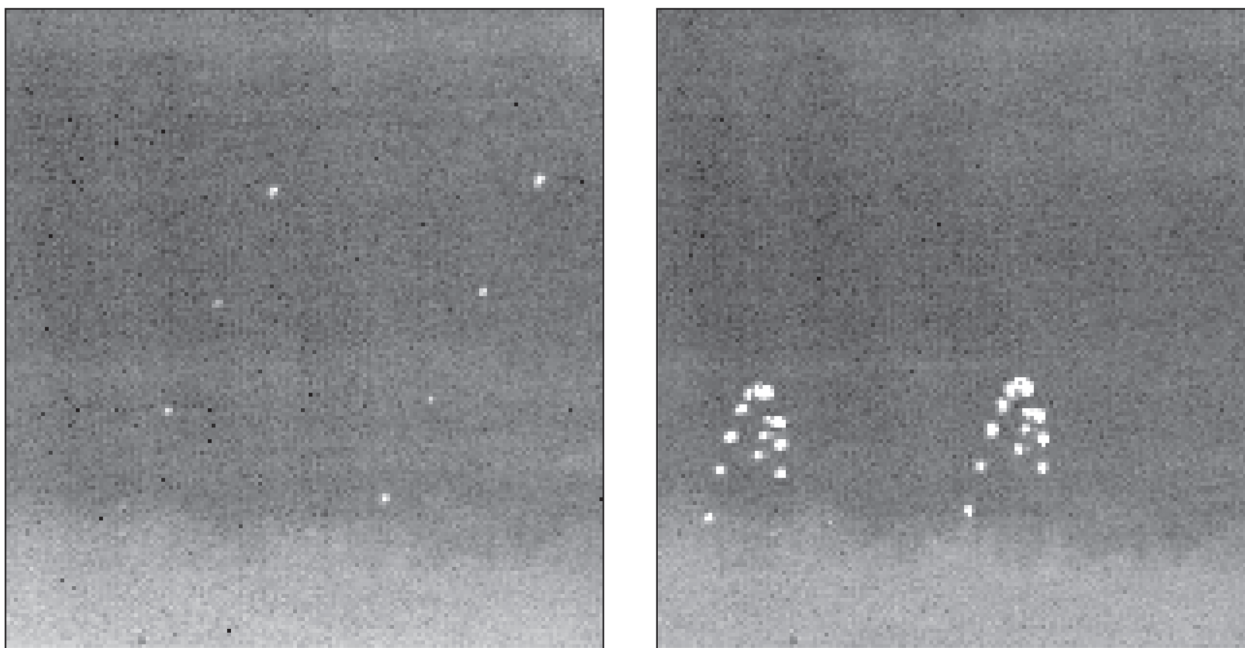


**Figure 10.** IR images of a model rocket (left) and magnesium flare (right) at a distance of about 5 nmi. Pairs of images result from superposition of two perspective images on the focal plane. Multiple images are overlaid on the figure.

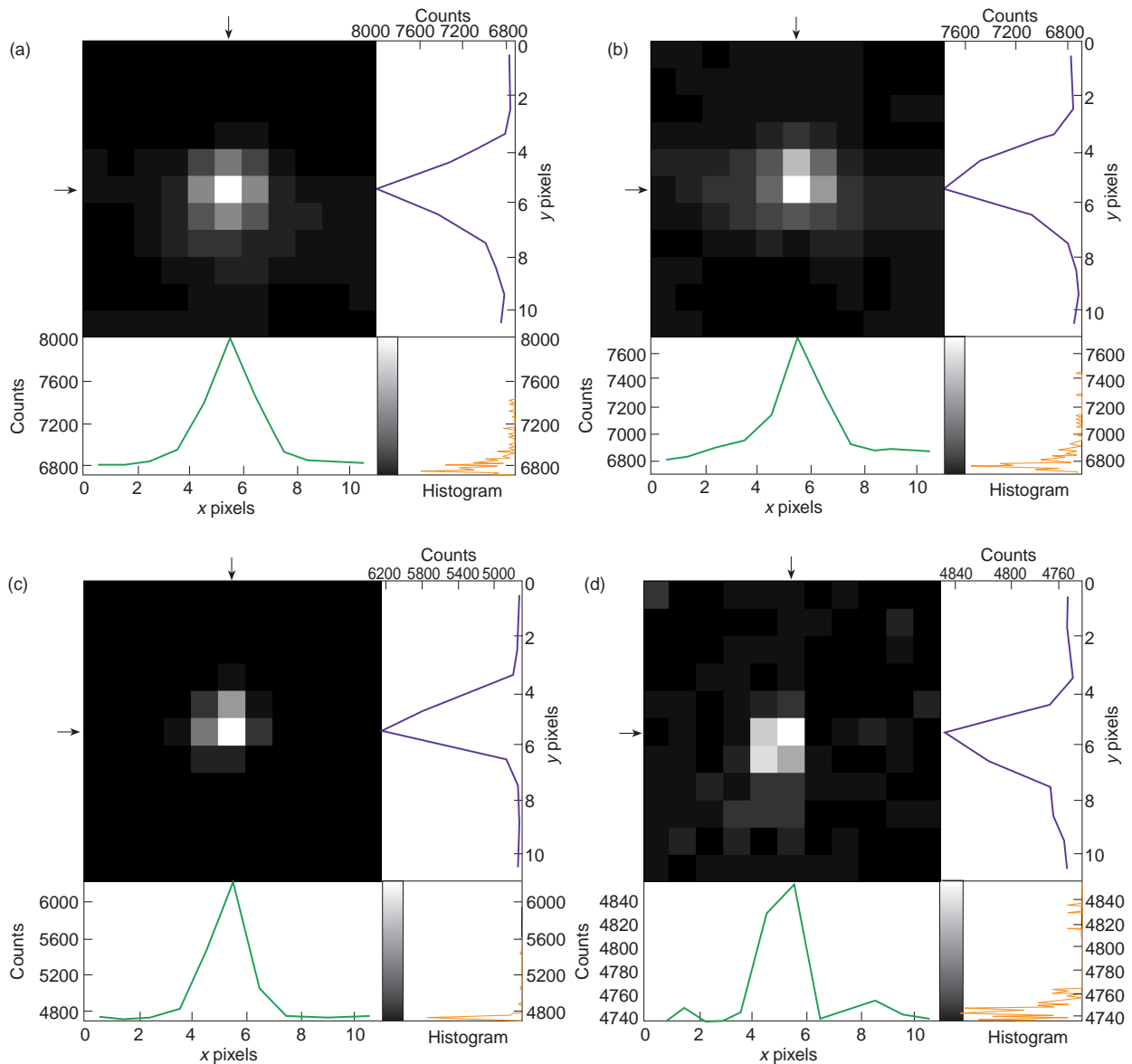


**Figure 11.** Sample IR images from test targets: (a) 20-in.-dia. calibrated source at 137°C and 3.2 nmi, (b) 500-W quartz lamp at 3.2 nmi, (c) magnesium flare at 4.9 nmi, and (d) model rocket at 4.9 nmi. A magnified image of 10 × 10 pixels is shown. Plots indicate similarity of sources with respect to radiance in the IR band and spatial distribution of energy.

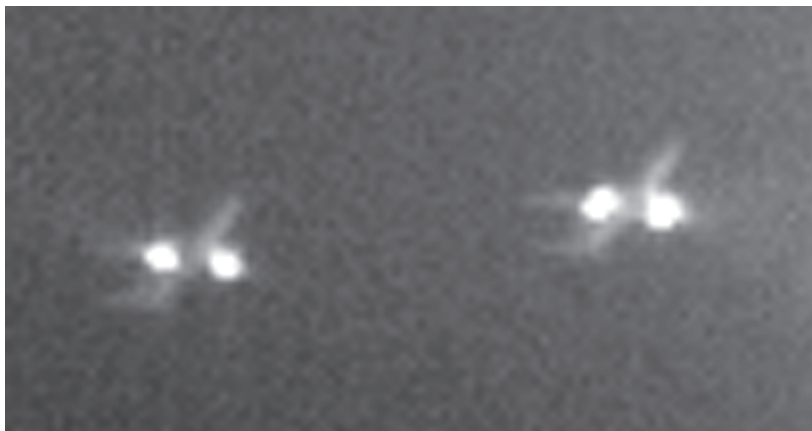


**Figure 12.** Double image of an airliner at a 9-nmi range.

elevation. The radar range is taken as the “true” range standard. The AN/SPG-55B radar has a range error of less than  $\pm 25$  ft according to the manufacturer.

IR data were processed in the laboratory after the tests. At close ranges, extended targets were resolved (i.e., the aircraft subtended a number of pixels), and a prominent IR source on the aircraft was used for ranging. At distant ranges, all targets were unresolved, making the image equivalent to a point source as in Fig. 11.

Figure 13 shows examples of ranging performance for an inbound and outbound Cessna. The black curves are plotted from radar data; the circles show IR range determined with a 16-point sliding window average. Our averaging process is not an optimum one: samples were taken over a relatively long sampling interval during which measurable target motion may have occurred. Increased data rates and advanced filtering/prediction algorithms such as Kalman filtering are expected to improve range estimates.

Figure 13 shows that the IR range tends to degrade as the target range increases, in accordance with theoretical expectations (Eq. 1). The experimental relationship between accuracy and range is shown in Fig. 14, which displays range error versus range. Using data collected over the range interval from 4 to 20 nmi, the following regression formula was obtained:

$$E = 0.27R + 1.0 \quad (4)$$

where  $E$  is the range error (in percent) and  $R$  is the range (in nmi). These results are drawn from 2 days of testing consisting of 30 airborne target encounters.

### Calibration Angle Drift

Previously, we noted that deviations in the pentamirror angle could be attributed to thermal gradients across the pentamirror structure caused by solar heating. We also described how rotations of the optics about certain axes can couple into the target separation angle. These effects appear as a “calibration angle drift,” in which the apparent difference angle ( $\theta_1 - \theta_2$ ) to a fixed target seems to vary with time. The effect is significant, resulting in a range error as large as 70% at 17 nmi. For range measurements reported in this article, we have overcome the problem with frequent recalibration.

For the next prototype model, we are attempting to mitigate this problem with solar shields on critical components and a more rigid baseline structure. For a shipboard system, we expect to enclose these components in an air-conditioned housing. Further tests will be needed to ensure that the problem of calibration drift has been adequately addressed by these procedures. If periodic recalibration is required, it could be performed using an IR source positioned on the ship or by using a target of opportunity in the vicinity of the ship with a known range.

For the next prototype model, we are attempting to mitigate this problem with solar shields on critical components and a more rigid baseline structure. For a shipboard system, we expect to enclose these components in an air-conditioned housing. Further tests will be needed to ensure that the problem of calibration drift has been adequately addressed by these procedures. If periodic recalibration is required, it could be performed using an IR source positioned on the ship or by using a target of opportunity in the vicinity of the ship with a known range.

### FUTURE DEVELOPMENT AND APPLICATIONS

We have constructed the ranger configuration shown in Fig. 15. Two pentamirrors are placed symmetrically about the central reflector that redirects ray paths by 90°. Compared with the arrangement in Fig. 4, the newer design uses an additional optical element (the 90° reflector). One advantage of the symmetrical design is that the most

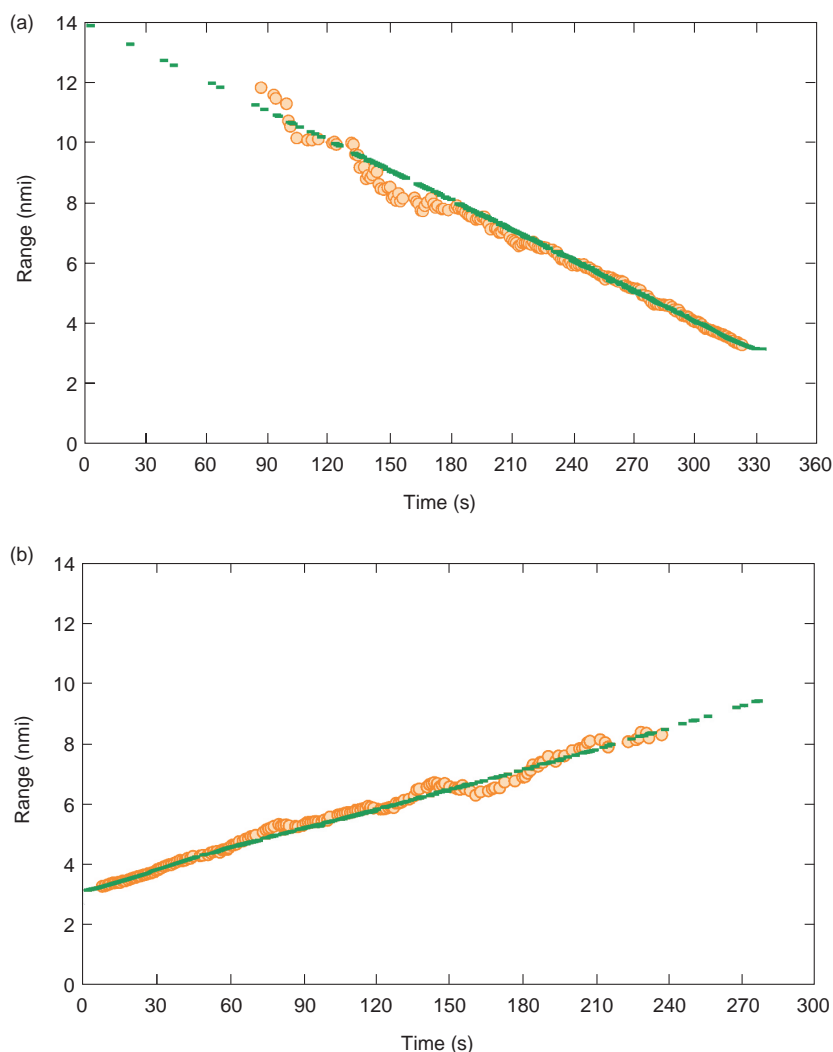


**Figure 13.** IR ranging performance compared with radar range for two Cessna encounters: (a) inbound and (b) outbound. Circles indicate sliding window of 16-point averages, with data rate at 2 frames per second. Green data points were plotted from radar range data.

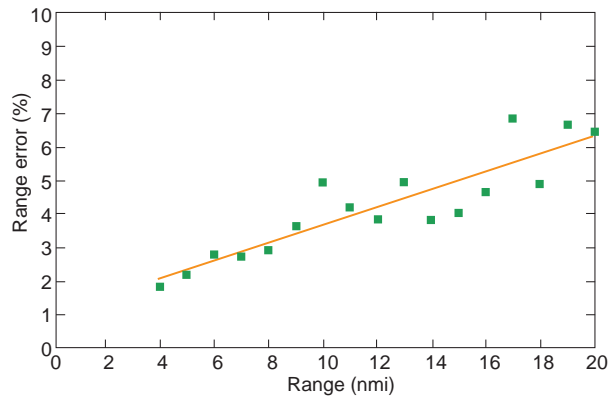


**Figure 14.** Measured passive ranging performance. The curve indicates the regression/trend line.

massive units are placed closer to the center of the device. This should reduce the mechanical moment of inertia, which would be an advantage in a steerable system. A disadvantage of this design is that it requires an additional optical element, which introduces a greater possibility for optical irregularities, signal loss, and angle errors due to vibration and bending. Although we do not think that these will be serious limitations, further testing will be required to prove the concept.

The symmetrical design (Fig. 15) uses a lattice framework for the baseline and solar shields for thermal stability. This second-generation prototype ranger is attachable to an Mk-99 illuminator. It is expected to be much lighter and more rigid than the current test model by virtue of the lattice framework.

We are designing the new version to have an 8-ft baseline, as opposed to 10 ft for the first-generation

prototype, to reduce the rotational inertia and dynamic loading on the illuminator pedestal. As suggested by Eq. 2, the shorter baseline would result in an increased range error by the factor 1.2. This increased error can be compensated for by increasing the number of samples used for averaging from 16 to 25. Such an increase should be acceptable, considering that the new version will also use a much faster sampling rate.

A subsequent stage of construction will be required for shipboard testing (Fig. 16). The new version will have to be protected from adverse weather conditions and ship vibration. A further improvement will include means for preventing wind-driven salt spray from reaching the sensitive elements of the ranger. We are considering enclosure designs that use either a forced-air baffle concept or optical windows at the pentamirror access ports.

Again, we envision that before the system would become fully operational and deployed, the target image localization and range calculations will be automatic and occur in real-time. The ranger concept described here is best suited for a system that is cued or directed at potential threats by other sensor systems (i.e., radar or scanning IR sensors) that perform initial target detection. The ranger will then provide target location information to assist with tracking and weapons direction.

Although the development of the IR passive ranger has been focused on naval defense, it has many other possible functions, e.g., unmanned aerial vehicles, ground forces target ranging, harbor navigation, general surveillance, and civilian traffic management. Any situation that requires range (or range

rate) to an object with thermal contrast could benefit from an IR ranger. The dimensions of the ranger can be adjusted to best suit the expected target ranges. One significant attribute of the IR ranger is its completely passive nature; no energy is emitted to measure range and angular position. This could be especially important for certain military and surveillance applications.

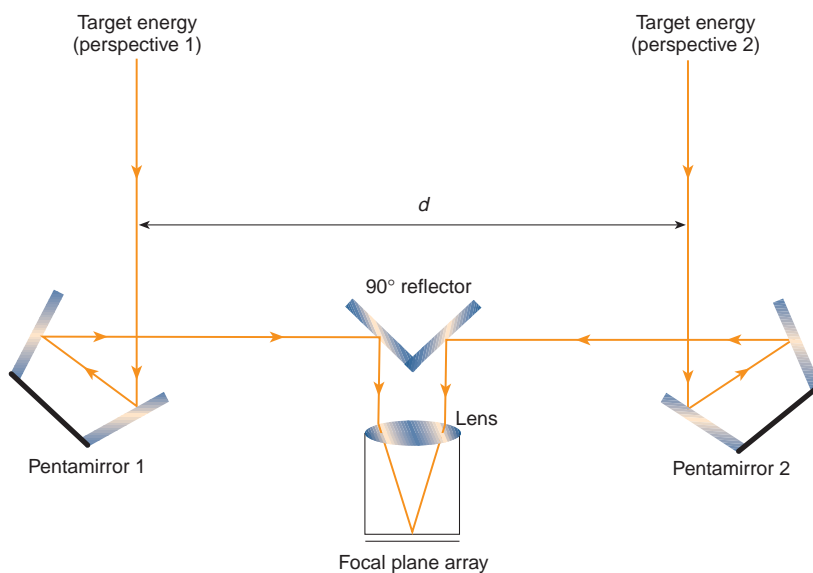


**Figure 15.** Passive ranger concept with symmetrical layout. Pentamirrors define the baseline  $d$  (8 ft). An additional 90° reflector redirects energy to the camera, which is located between the two pentamirrors.

## CONCLUSIONS

We have demonstrated a method for passively determining range to an IR target. With the design described here, an accuracy of a few percent is possible out to ranges of 15 nmi or so—effectively the limits of the optical horizon for a

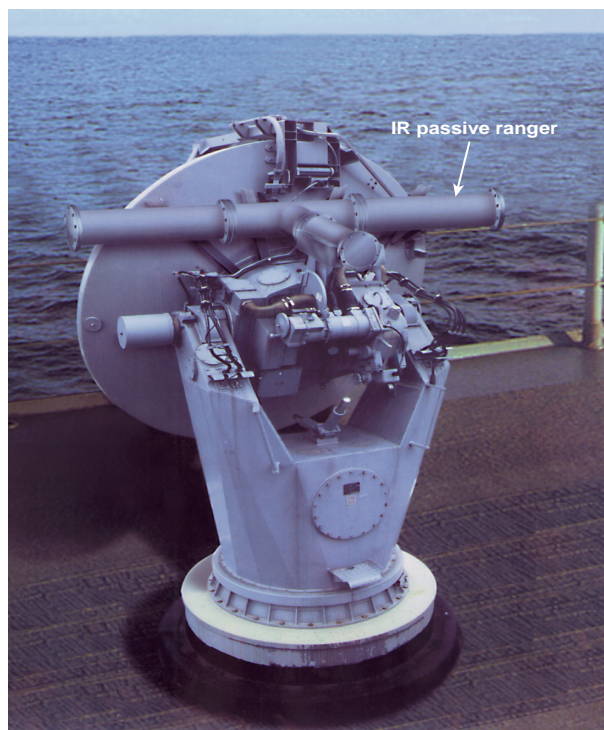


**Figure 16.** Shipboard testing of the ranger is a future goal. A hypothetical test arrangement is shown attached to an Mk-99 illuminator.

low-altitude target. Our design uses stereo imagery with a single lens, camera, and focal plane. The use of pentamirrors eliminates a major error source involving optical alignment within the system.

We have completed a prototype that is lighter and more compact, and should be more accurate. Modifications are expected to eliminate the need for frequent calibration.

After testing this prototype in a seashore environment, the next major phase will involve the development of a unit suitable for shipboard testing. This unit will require measures to accommodate the vibration and salt spray insults that are expected on a

ship-deployed unit. A major technical challenge will be the development of a real-time processing capability.

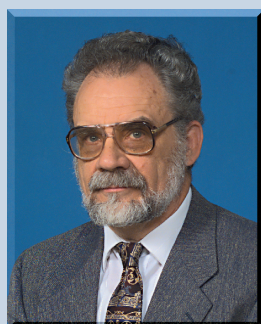
Clearly, the passive ranger design discussed here is a practical one that fully achieves all our objectives with existing technology. Although the development of the ranger has been focused on naval defense, many other potential applications exist.

#### REFERENCES

- <sup>1</sup>Reilly, J. P., Younkins, L. T., and Taylor, R. J., "Infrared Passive Ranging Using Sea Background for Accurate Sensor Registration," *Proc. SPIE* **2469**, 318-329 (1995).
- <sup>2</sup>Reilly, J. P., Younkins, L. T., and Taylor, R. J., *Accurate Alignment of Stereo Cameras Using Images of Earth or Sea Surface Features*, Invention Disclosure 1263 (26 Apr 1995).
- <sup>3</sup>Nelson, C. V., Taylor, R. J., and Klein, T. L., *Investigation of Airborne Target IR Passive Ranging Using Photogrammetry*, STR-95-084, JHU/APL, Laurel, MD (1995).
- <sup>4</sup>Ilves, H., and Reilly, J. P., *Infrared Passive Ranger Using Triangulation, One Sensor, and Two Pentamirrors*, Invention Disclosure submitted to APL Patent Office (19 Jun 1997).
- <sup>5</sup>Kohler, D. R., *Errors Due to Misalignments in a Range Finder*, STX-97-139, JHU/APL, Laurel, MD (1997).
- <sup>6</sup>Klein, T. L., *Correction of Geometric Lens Distortion*, STS-97-173, JHU/APL, Laurel, MD (1997).
- <sup>7</sup>Klein, T. L., and Reilly, J. P., *Infrared Scintillation in the 3-5  $\mu\text{m}$  Band in a Coastal Marine Environment: Theory and Measurements at Low Altitudes*, ADS-96-013/STD-B-0055, JHU/APL, Laurel, MD (Jan 1997).
- <sup>8</sup>Klein, T. L., and Reilly, J. P., "Characteristics of 3-5  $\mu\text{m}$  Scintillation at Low Altitudes in a Coastal Marine Environment," in *Proc. 1996 Meeting of the IRIS Specialty Group on Targets, Background and Discrimination*, Albuquerque, NM (30 Jan-1 Feb 1996).
- <sup>9</sup>Klein, T. L., *Angle-of-Arrival Fluctuations and IR Passive Ranging*, STS-98-074, JHU/APL, Laurel, MD (1998).
- <sup>10</sup>Klein, T. L., *Differential Refraction and IR Passive Ranging*, STS-98-073, JHU/APL, Laurel, MD (1998).

**ACKNOWLEDGMENTS:** The development of the passive ranger, from initial concepts to the present test unit, was carried out through the efforts of many people who participated in design, testing, and analysis. Major contributors included L. Wayne Elliott (PSI), David R. Kohler (STX), Carl V. Nelson (VSE), Joseph S. Peri (A3B), Robert J. Taylor (formerly APL, STR), Lloyd D. Tubbs (STR, retired), and Larry T. Younkins (A3B). In addition, many people provided significant technical support, including David R. Frostbutter (A1B), William R. Geller (A1B), James M. Hanson (A1B), Bryan C. Jacobs (PTP), James R. Kime (A1C), Bernard E. Kluga (A1B), Frank J. Marcotte (A1B), and Martin J. Pittinger (PTP). Dennis V. Webster and Richard Pregelman were strong advocates of the project during the IR&D phase. Mr. Webster was program manager when the project transferred to U.S. Navy support; he has made many technical contributions as well. We owe a debt of appreciation to the Cessna pilot (D.R. Frostbutter) and attendant (W. R. Geller) who endured freezing temperatures in an open cockpit to position the IR source. Thanks also go to Gerard Balkcom (PTP) for his efforts in acquiring the surplus (yet very valuable) pentamirrors and to Anthony Krenzer and Matthew Baughman for technical illustrations.

#### THE AUTHORS



J. PATRICK REILLY obtained a B.E.E. from the University of Detroit in 1962 and an M.S.E. from George Washington University in 1965. Since joining APL in 1962, he has worked on a variety of theoretical and experimental projects associated with radar, sonar, acoustics, IR systems, and bioelectric phenomena. He initiated and directed the IR passive ranger project from its IR&D phase to the stage of development described in this article. Mr. Reilly recently retired as a full-time Principal Professional Staff member after serving as the supervisor of the Environmental Modeling Section of the Air Defense Systems Department. He was the director of research programs on human reactions to electric currents and electromagnetic fields. Mr. Reilly is a senior member of the IEEE and a member of the Bioelectromagnetics Society. He has written one book, *Electrical Stimulation and Electropathology*, co-authored another, *Radar Design Principles*, and his newest book, *Applied Bioelectricity*, is in press. His e-mail address is patrick.reilly@jhuapl.edu.



TROY KLEIN received his B.S. degree in engineering physics from the University of Illinois at Urbana-Champaign in 1990 and his M.S. degree in electrical engineering from The Johns Hopkins University in 1996. Since joining APL in 1990, Mr. Klein has worked with a wide variety of sensor systems and data including synthetic aperture radar, passive visible and infrared optics, active visible optics, and active underwater acoustics. Through his involvement with these systems, he has expertise in signal and image processing, statistical data analysis, modeling, optics, and experimental measurements. His activities for the IR passive ranger project included designing, developing, and applying the image processing and ranging software; operating the image acquisition hardware; and performing many theoretical and modeling studies. Mr. Klein is a member of APL's Senior Professional Staff in the Signal and Information Processing Group of the Submarine Technology Department. His e-mail address is troy.klein@jhuapl.edu.



HILLAR ILVES received a B.A. in physics from Alfred University in 1962 and an M.S. in electrical engineering from Colorado State University in 1965. Before joining APL in 1972, he worked for ARPA at the Military Research and Development Center in Bangkok, Thailand, from 1965 to 1967. From 1967 to 1972, he taught physics and mathematics and initiated the computer science department at Franklin Pierce College. Mr. Ilves's work at APL has focused on Poseidon, Polaris, and Trident guidance prelaunch analysis and evaluation. More recently, and until his retirement in 1997, his interests included application of quantum optics to encryption, photonics, interferometry, and electro-optic crystals. He also served as technical lead for the IR passive ranger project, designing the optical systems, constructing and developing the ranger instrument, and conducting the tests described in this article. He is a co-recipient of APL's R. W. Hart Prize for Excellence in Research. Mr. Ilves is the inventor of a two-degree-of-freedom torsion plate mount and co-inventor of the IR passive ranger described in this article.